MID-AMERICA
TRANSPORTATION CENTER

Report # MATC-UI: 145-2

Final Report
WBS:25-1121-0005-145-2

Real-Time Flood Forecasting for River Crossings - Phase II

Witold Krajewski, PhD
Rose & Joseph Summers Chair in Water Resources Engineering
Faculty Research Engineering, IIHR - Hydroscience Engineering
Director, Iowa Flood Center
The University of Iowa

Ricardo Mantilla, PhD
Assistant Professor
Research Engineer, Iowa Flood Center
Department of Civil and Environmental Engineering
The University of Iowa

2020

A Cooperative Research Project sponsored by
U.S. Department of Transportation- Office of the Assistant Secretary for Research and Technology

Real-Time Flood Forecasting for River Crossings – Phase II

Witold Krajewski, PhD, P.I.
Rose & Joseph Summers Chair in Water Resources Engineering
Faculty Research Engineer, IIHR - Hydroscience & Engineering
Director, Iowa Flood Center
The University of Iowa

Ricardo Mantilla, PhD, P.I.
Assistant Professor
Research Engineer, Iowa Flood Center
Department of Civil and Environmental Engineering
The University of Iowa

A Report on Research Sponsored by

Mid-America Transportation Center

University of Nebraska–Lincoln

January 2020

Technical Report Documentation Page

1. Report No. 25-1121-0005-145-2	2. Government Accession No.	3. Recipient's Catalog No.
4. Title and Subtitle Real-Time Flood Forecasting for River Crossings		5. Report Date January 2020
		6. Performing Organization Code
7. Author(s) Witold Krajewski, PhD ORCID: 0000-0002-3477-9281 Ricardo Mantilla, PhD ORCID: 0000-0002-2957-6252		8. Performing Organization Report No. 25-1121-0005-145-2
9. Performing Organization Name and Address Mid-America Transportation Center Prem S. Paul Research Center at Whittier School 2200 Vine St. Lincoln, NE 68583-0851		10. Work Unit No. (TRAIS)
		11. Contract or Grant No. 69A3551747107
12. Sponsoring Agency Name and Address Office of the Assistant Secretary for Research and Technology 1200 New Jersey Ave., SE Washington, D.C. 20590		13. Type of Report and Period Covered Final Report, November 2019 – December 2019
		14. Sponsoring Agency Code MATC TRB RiP No. 91994-39
15. Supplementary Notes		
16. Abstract We have developed a generic prototype of a flood-forecasting model that is transferable to other locations around the Midwest to provide monitoring and forecasting flood potential at critical infrastructure points, such as bridges, where streamflow gauges are not available. A real-time web-based visualization platform to display the model predictions has been implemented. The platform will display the river network upstream from a point of interest and a time control slider that will allow exploring the evolution of flows everywhere in the network over the past several days, and about a week into the future. The model uses in-house developed radar-rainfall maps updated every 5 minutes with the spatial resolution of about 0.5 km currently covering the Iowa domain and extending some 100 km into the neighboring states. For the future rainfall, we use predictions for the National Weather Service High-Resolution Rapid Refresh (HRRR) forecasting system. The system provides hourly accumulation products for up to 20 hours ahead. Our system expands the forecasting capabilities of the current NWS by providing predictions at locations that have not been historically gauged.		
17. Distribution Statement		

18. Security Classif. (of this report)	19. Security Classif. (of this page)	20. No. of Pages	21. Price
Unclassified	Unclassified	39	

Table of Contents

List of Figures

List of Tables

List of Abbreviations (optional)

Mid-America Transportation Center (MATC)
Nebraska Transportation Center (NTC)

Disclaimer

The contents of this report reflect the views of the authors, who are responsible for the facts and the accuracy of the information presented herein. This document is disseminated in the interest of information exchange. The report is funded, partially or entirely, by a grant from the U.S. Department of Transportation's University Transportation Centers Program. However, the U.S. Government assumes no liability for the contents or use thereof.

Abstract

We have developed a generic prototype of a flood-forecasting model that is transferable to other locations around the Midwest to provide monitoring and forecasting flood potential at critical infrastructure points, such as bridges, where streamflow gauges are not available. Our efforts have centered around creating tools and protocols that would facilitate the implementation of the hydrological model in any of the four MATC states. The protocols include 1) a methodology to use existing regional data to determine the parameters in the runoff routing equation along the river network, 2) a methodology to determine the infiltration parameters that control rainfall-runoff transformation, and 3) a new set of equations that are more appropriate to simulate subsurface runoff from artificially drained landscapes (agricultural tiled landscapes). Also, a new web based graphical user interface has been developed to evaluate the model performance at multiple locations and to compare different model configurations. The interface also allows for intercomparing different hydrological models.

Chapter 1 Preliminaries: The Iowa Flood Center HLM hydrological model

The Iowa Flood Center hydrological model, Hillslope-Link Model (HLM), is a distributed hillslope-scale rainfall-runoff model that partitions Iowa into over three million individual control volumes following the landscape decomposition outlined in Mantilla and Gupta (2005). The model is parsimonious, using ordinary differential equations to describe transport between adjacent control volumes. This characteristic reduces the computational resources needed by capturing the most essential features of the rainfall runoff transformation; it uses only a few parameters to obtain acceptable results. The model partitions the river network into river links (the portion of a river channel between two junctions of a river network) and the landscape into hillslopes (adjacent areas that drain into the links).

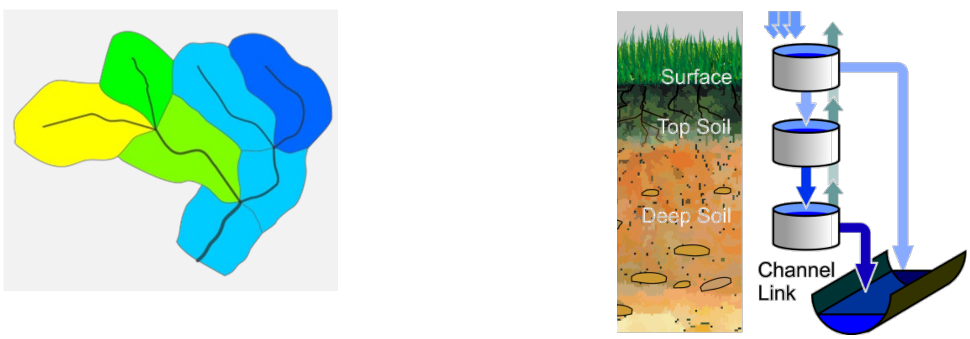

(a) (b)

Figure 1.1 (a) illustration of landscape decomposition into hillslopes and decomposition of the river network into channel link and (b) vertical soil profile and control volumes included in the hydrological model

Mass conservation equations give rise to the system of coupled nonlinear ordinary differential equations that represent changes in the water storage in the hillslope surface (s_{surf}), top soil (s_{tops}), and deep soil (s_{deeps}) given by,

$$
\begin{cases}
\dfrac{ds_{surf}(t)}{dt} = p(t) - q_{runoff}(t) - q_{infil}(t) - e_{surf}(t) & (1.1) \\
\dfrac{ds_{tops}(t)}{dt} = q_{infil}(t) - q_{percol}(t) - e_{tops}(t) & (1.2) \\
\dfrac{ds_{deeps}(t)}{dt} = q_{percol}(t) - q_{baseflow}(t) - e_{deeps}(t) & (1.3)
\end{cases}
$$

Fluxes in, across, and out of the vertical hillslope control volumes include precipitation $p(t)$, overland runoff q_{runoff}(t), infiltration into the topsoil q_{infil}, percolation from the topsoil into the deeper soils q_{percol}(t), baseflow into the channel $q_{baseflow}$(t), and evaporation from the ponded, topsoil, and deep soil layers (e_{surf}(t), e_{tops}(t) and e_{deeps}(t), respectively). The model assumes that percolation flux is a linear function of the amount of water stored at time t in the topsoil $q_{percol}=k_{percol}\cdot s_{tops}$ and that the baseflow is a linear function of the water stored in deep soil $q_{baseflow}=k_{baseflow}\cdot s_{deeps}$. Overland runoff is a power function of the water stored on the hillslope surface (consistent with Manning's equation) given by,

$$q_{runoff} = k_{runoff} s_{surf}^{1.67} \tag{1.4}$$

and infiltration is a nonlinear function of soil moisture content (s_{tops}/T_{tops}), where T_{tops} is the thickness of the topsoil layer (i.e., A-horizon) and a linear function of hydraulic head s_{surf} given by,

$$q_{infil} = k_{dry}\left(1 - \frac{s_{tops}}{T_{tops}}\right)^{\phi} s_{surf} \tag{1.5}$$

where k_{dry} corresponds to the case of dry soil and, similarly to k_{runoff}, k_{percol}, and $k_{baseflow}$ can be interpreted as time constant (residence time) of the respective storage component. The hillslope area (a_h) for the elements in the distributed model is, on average, 0.05 km², and link length (l_{link}) is, on average, 400 m. Note that $a_h/(2l_{link})$ is the hillslope length. The exponent φ is a nonlinearity introduced by the change in the potential matric of the soil column as soil moisture changes with time.

The HLM should be thought of as a modeling system rather than a single specific model. As the equations describing hillslope-scale processes are separated from the numerical solver, it is rather easy to explore different mathematical descriptions for water fluxes. For example, one can consider such simplifications as constant runoff coefficient or water transport velocity, or as an alternative, one can formulate these components based on the available physical characteristics.

Water transport through the river network is nonlinear and governs how channel links propagate flow through the river network. Formulated in the context of a mass conservation equation developed by Gupta and Waymire (1998), it uses the water velocity parameterization given by Mantilla (2007) as,

$$\frac{dq_{link}(t)}{dt} = \frac{v_0 q_{link}^{\lambda_1}(t) A^{\lambda_2}}{(1-\lambda_1)l}\left[a_h\left(k_{runoff} s_{surf}^{1.67}(t) + k_{baseflow} s_{deeps}(t)\right) - q_{link}(t) + q_1(t) + q_2(t)\right] \tag{1.6}$$

where q_{link} is the discharge from the link at time t, a_h is the total hillslope area draining to the link, $q_1(t)$ and $q_2(t)$ are the incoming flows of the upstream tributaries, A is the upstream basin area, and λ_1, λ_2, and v_0 are global parameters of the water velocity component of the model and are set to 0.2, -0.1, and 0.3, respectively. The model can capture the main features of the hydrographs including the maximum stage. We used the model in several studies (e.g., Ayalew et al. 2014; Cunha et al. 2012). We also discuss the model performance in Krajewski et al. (2017). The model is driven by radar-rainfall estimated from Level II NEXRAD data from seven WSR-88D weather radars covering the state of Iowa. The maps of rainfall intensity have spatial resolution of about 0.25 km^2 and are updated every five minutes. The algorithms are described in Krajewski et al. (2013) and Seo and Krajewski (2015).

An important aspect of our modeling approach is the avoidance of calibration. Instead, we rely on detailed information of the physical properties we model. This includes the topography, land use and land cover, soil properties, and details of the main forcing, i.e., precipitation. Comparing simulation results to streamflow observations across Iowa validates the model formulation and parameterization. Therefore, we can view the model as data-intensive and calibration-free when used in forecast-mode. This, in turn, implies that with more detailed, relevant, and accurate data, including model states and physical domain characterization as well as the driving inputs, the model will work better. The model is fully automatic in the sense that no corrections are applied to the model as it moves forward in time once initial and boundary conditions are imposed.

The model predicts the streamflow fluctuations associated with storm events over the catchment of interest using current observations of rainfall, and rainfall forecasts. The effect of storms on river ways is usually delayed ranging from days to weeks. Each point of interest in the landscape (bridge, culvert) can then be categorized according to the maximum warning time. The web interface will provide a visual tool to show when a particular location will be impacted, and it will provide an inundation map associated to the particular peak flow expected for that location. Inundation maps are more effective tools in communicating the effects of flooding than crest stages at specific locations.

Chapter 2 Developing a data approach for the model parameterization, routing case

The HLM model has an overall satisfactory performance, however, the set of parameters chosen for Iowa are not expected to be universal, and therefore the parameters to be used in other regions need to be calculated. Typically, parameters are obtained through model calibration (Devia et al., 2015; Moussa et al., 2009), which has issues. Calibration is usually done at the outlet of the basin, leaving potential uncertainties at the sub basins. Also, this procedure could lead to physical inconsistencies in the models. Considering this, we propose a data approach to obtain the parameters of the model at a regional scale. Unlike the classical calibration, the data approach obtains the parameters of the model from emerging patterns presented at the observed data (Sivapalan, 2018). In this case, we apply the approach to the parameters of the routing equation; however, it could be expanded to other parameters of the model. Our implementation starts extracting the parameters from the smallest basins with streamflow records in the region and ends extrapolating the same parameters for all the model domain.

2.1 Methodology

For the approach, we first select the base data set corresponding to 51 USGS streamflow gauges of basins with areas below 1300 km^2 (red dots in Figure 2.1). The base data correspond to relatively small watersheds because their internal parameter variability is likely to diminish compared to basins with more area. From this data, we first run an experiment to obtain the dominant routing parameters. Then we explore two interpolation approaches to assign those parameters for the model domain. Finally, we evaluate the obtained results for all the stations (blue and red dots in Figure 2.1)

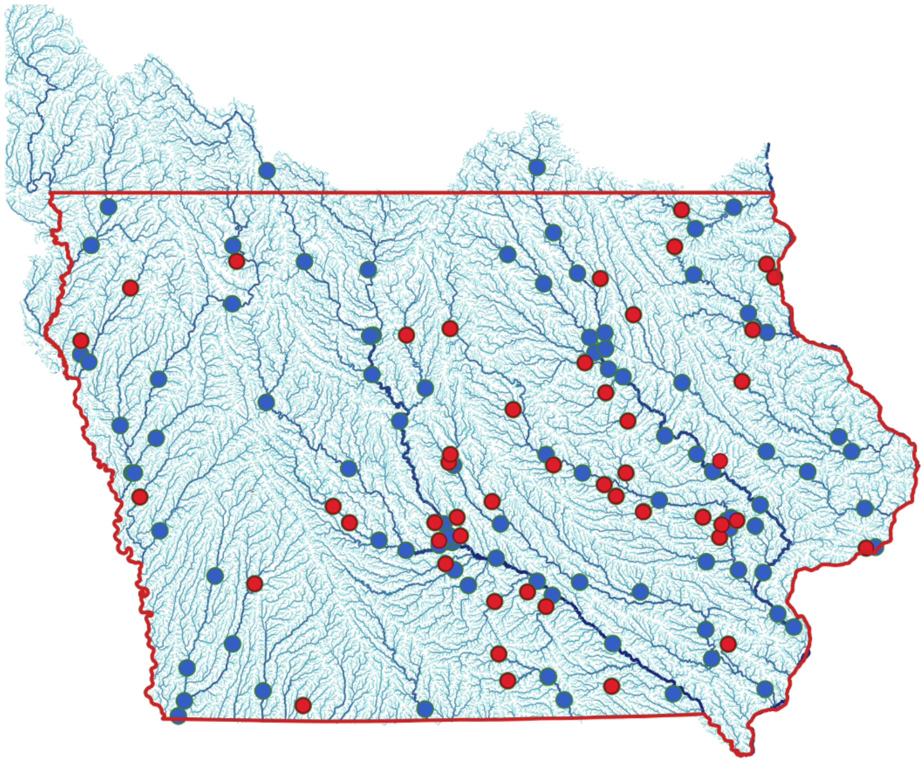

Figure 2.1 USGS streamflow stations used for the data-based approach (red) and for the validation of the results (blue).

At the base data set, we evaluate nine combinations of the parameters that mostly control the model routing scheme λ_1 and v_0. For this, we identify the rainfall-runoff events, and in each, we run a time-step runoff-controlled ODE hillslope model. In this setup of the model, we first make executions of the model with multiple RC values in a window of time of three hours (dt_m in figure 2.2a). Then, we continue running each realization without rainfall for a time window of six hours (dt_n in figure 2.2a). At the end of the second window, we compare the total simulated and observed streamflow volumes and select the streamflow and initial conditions from the RC setup with a lower difference (end of step figure 2.2a). Then, we repeat this procedure until the end of the observed hydrograph (figure 2.2b and c). In figure 2.3 we present an example of the results obtained for an event at the USGS station 06600100. Using the described procedure, we correct the simulated volume for each combination of λ_1 and v_o and for each watershed we select the combination with the best performance in most events.

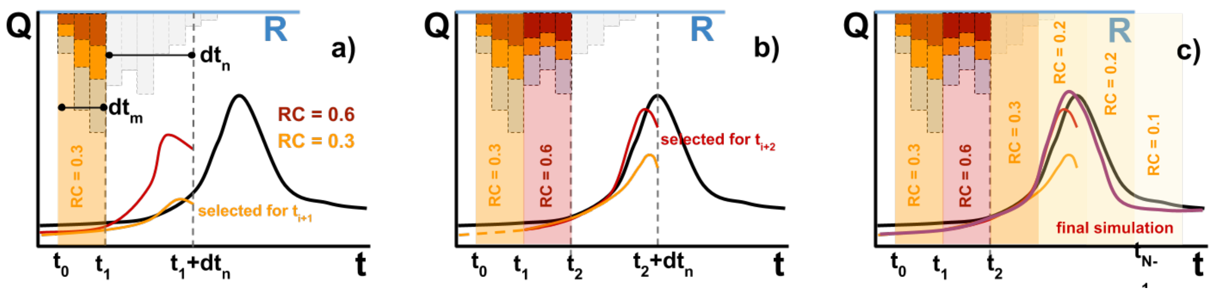

Figure 2.2 Time-step controlled runoff strategy. From left to right, the figure presents a typical evolution of the model identifying the correct RC for a certain routing parameter combination.

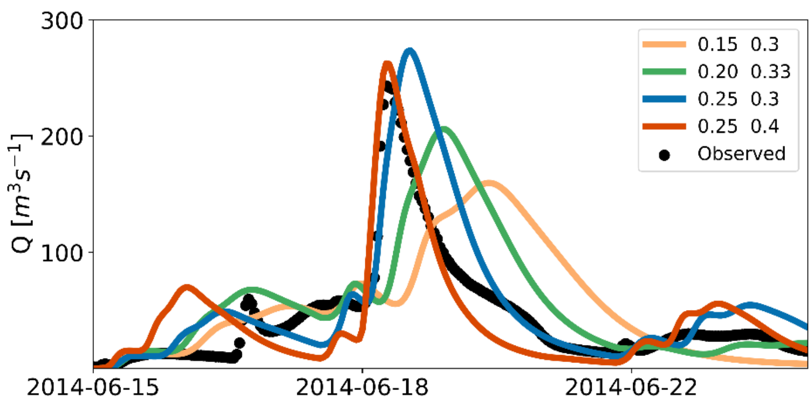

Figure 2.3 Results of the time-step runoff-controlled ODE model applied for an event at the USGS station 06600100.

After finding the combinations at the small basins, we interpolate our results to all the links in the domain of the model. For this, we use a simple interpolation approach that we called nested HUCS (n-HUCS), and a more complex one, Random Forest (RF). We choose two methodologies of different complexity levels to be able to contrast the influence of the spatial distribution of the patterns. Then, we run the model from 2012 to 2018 and compare the results for all 138 USGS stations with good quality records in Iowa (blue dots at figure 2.1). Finally, we evaluate the differences in terms of the KGE index (Gupta et al., 2009), the PFD, and the PTD.

The n-HUC method is iteratively applied over the HUCS of the region, starting with HUCS level 8 (fig. 2.4a) and finishing with HUCS level 2. In each iteration, the method calculates the group that has more occurrences inside each HUC (if there is any inside the HUC). Then, it assigns λ_1 and v_0 of the dominant group to the unclassified links of the HUC. With the decrease of the HUC level, we make sure that all the links of the domain have a λ_1 and v_0 value.

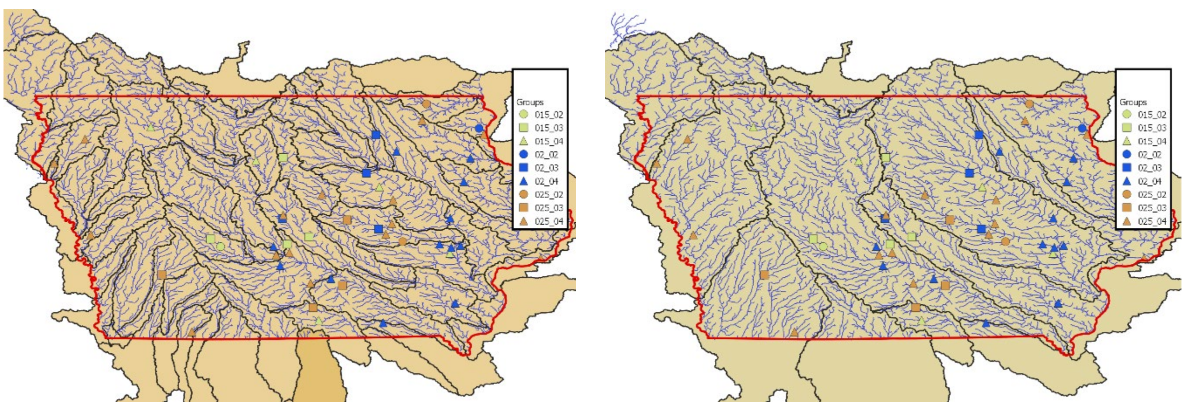

a) HUCS level 8 b) HUCs level 6

Figure 2.4 Example of the HUCS used for the interpolation of the parameters λ_1 and v_0. Left: HUCs level 8, right: HUCs level 6.

On the other hand, we applied the RF method, which involves more complexity. RF (Kam Ho, 1995) is a method part of the machine learning and data mining family, commonly used for supervised learning, clustering, classifications, and regressions. For its operation, RF takes decisions based on multiple Decision Trees (DS), each one trained to fit or classify data based on several inputs. Both, at the training and prediction, the RF outputs are the modal value of the results obtained by each DS. With this approximation, RF avoids overfitting, which is a common problem in the machine learning methods (Ali et al., 2012).

Each decision tree works by partitioning the data into "branches" or subsets that contain similar values (Quinlan, 1986). To achieve its goal, DS uses the "Bagging" training algorithm (Breiman, 1994). The pseudocode of a DS has three steps: 1) Place the best attribute of the data set (inputs) as the "root" of the three (squares leveled as I in figure 2.5), 2) Split the training set into subsets that become the first level of ramification, and 3) Repeat steps 1 and 2 on each subset until "leaf nodes" (green squares in figure 2.5) for all the branches can be found.

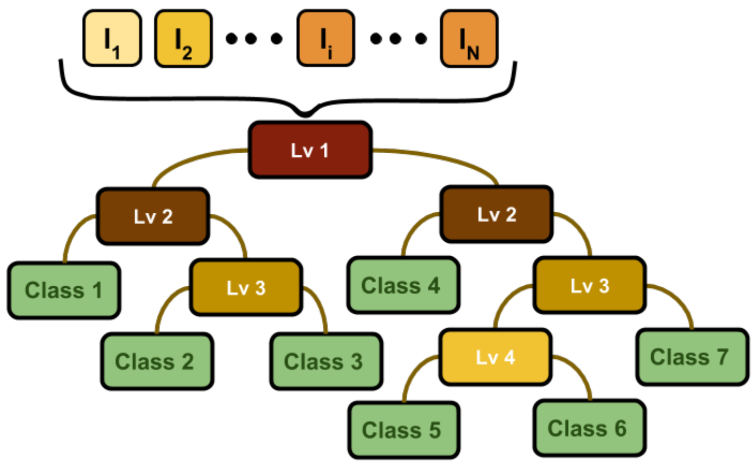

Figure 2.5 Schematic representation of a random forest that classifies inputs I_i into several classes (green squares).

For the setup of our experiment, we use the Random Forest class from the Python package Scikit-learn (Pedregosa et al., 2012). After trying several configurations, we use an RF with 20 estimators (DS), a max depth of 14 iterations, and a minimum of two samples per leaf. The input sample corresponds to nine hydrological features of each link, corresponding to the watersheds selected to obtain the combinations of λ_1 and v_0. The output sample is the obtained groups of λ_1 and v_0 numbered from 1 to 9. To avoid overfitting and biases, we train 400 different setups of RFs; in each case, we randomly select 70% of the sample for training and

30% for testing. We use three functions to evaluate the performance; the mean square error (MSE), the mean squared error of the pdf (MSEpdf), and the F1 score index (Sasaki, 2007). The MSE (equation (2.1)) accounts for the total number of hits of the RF, and its low value represents a good fit of the classification; however, its only use could lead to biases on the results. On the other hand, the MSEpdf stands for the mean error obtained by comparing the simulated and observed PDFs; we include this function to avoid bias in the selection of the best RFs. Finally, the F1 score is a popular accuracy metric used to evaluate classification performance.

$$MSE = \frac{1}{N}\sum_{i-1}^{N}\left(Y_i - \widehat{Y_\iota}\right)^2 \tag{2.1}$$

The F1 score uses the harmonic mean to emphasize the lowest value between the precision P and the recall R. Both metrics, P and R, are measurements extracted from the confusion matrix (error matrix) (figure 2.6). The precision defines how many selected items are relevant (equation (2.2)), while the recall says how many relevant items are selected (equation (2.3)). F1 is computed using equation (2.4) after P and R, F1 oscillates between 0 (worse model) and 1 (perfect model). With the usage of F1 we search for the model that has a high rate of true positives (TP) with a low amount of False Negatives (FN).

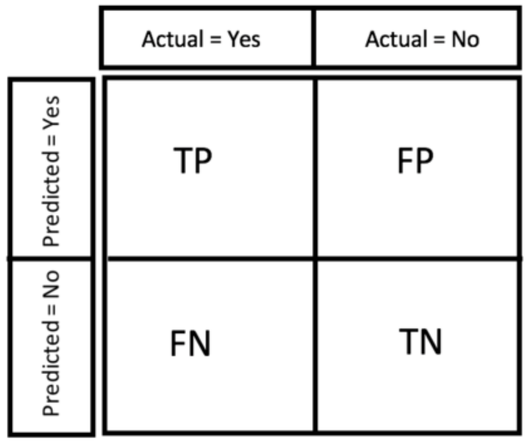

Figure 2.6 Confusion matrix, columns correspond to true and false observations, rows correspond to true and false predictions.

$$P = TP/(TP + FP) \tag{2.2}$$

$$R = TP/(TP + FN) \tag{2.3}$$

$$F1 = 2\,\frac{P \cdot R}{P + R} \tag{2.4}$$

To perform the interpolation, we select multiple RFs based on the described performance functions. We choose the realizations that are inside the first ten optimal surfaces obtained by comparing the functions applied to the test data (fig. 2.7a and b). Despite the competition among the functions, there is an overlap when we compare the selected realizations (yellow dots in figure 2.7) with the selected realizations from the contrary optimums (brown dots). Due to this shared behavior, we select all the optimal realizations from both comparisons (74 yellow dots). Finally, the interpolated value for each link is the modal value obtained by the selected RFs. With the selection of multiple RFs instead of one, we avoid mistakes due to the sample selection and obtain a more robust interpolator.

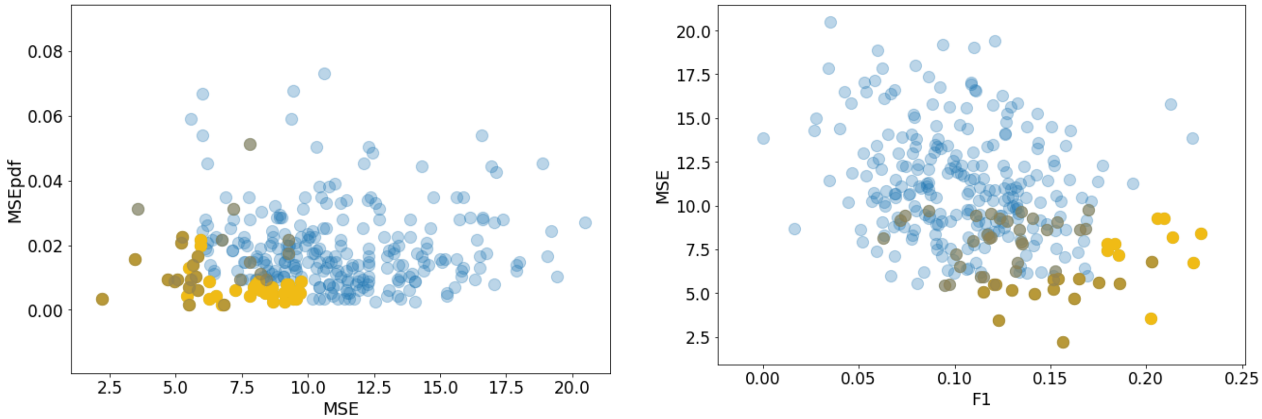

a) MSE vs MSEpdf space.

b) F1 vs MSE space.

Figure 2.7 Selected realizations of RF. Yellow dots stand for the RF realizations inside the first 10 optimal surfaces (selected RF). Brown dots correspond to the selected RF at the contrary space.

Additionally, we analyze the relevance of the input parameters for the RF in function of both surfaces (fig. 2.8a and b). In both cases, the slope (So), the HUC-8 category, and the travel time (Tt) are among the most relevant parameters. The total area (Λ), the total length of channels (Lt), and the total number of links (Nt) are in a second group. Finally, the less relevant parameters for all the cases are the watershed order, and the HUC-6 level.

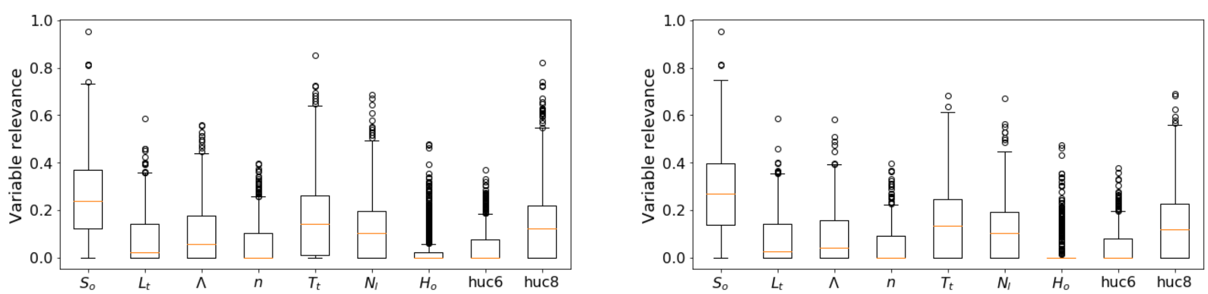

a) MSE vs MSEpdf

b) F1 vs MSE.

Figure 2.8 Input parameters relevance obtained by the RFs selected from the comparison of the objective functions.

2.2 Results and discussion

We first evaluate the performance of the time-step runoff-controlled ODE hillslope model. For this, we compare the simulated and the observed peak flows in the events used to obtain the best combinations. In figure 2.9a we present the results obtained using the best combination for each event. According to this result, our proposed methodology achieves to correctly simulate the peak flow magnitude at most of the events, with differences below the 20% for 221 cases out of 490. This performance diminishes when we simulate all the events with the best combination for the watershed (fig. 2.9b), in this instance, the cases with differences below the 20% is 127. However, the overall comparison still shows a good performance for the selected λ_1 and v_0 of each watershed.

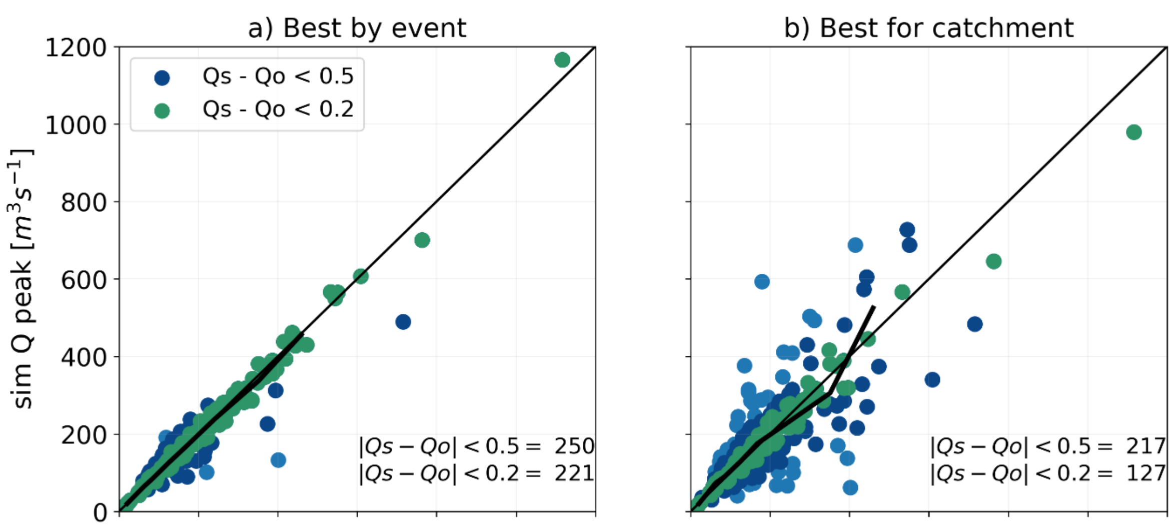

Figure 2.9 Observed versus simulated peak flows for the training set events. a) Comparison of the result of the best λ_1 and v_0 combination for each event, b) Comparison of the best combination by watershed.

Using two different methodologies, we interpolate λ_1 and v_0 for all the hydrological links of Iowa. In both cases, the base links were the ones corresponding to the small watersheds with

USGS streamflow records (fig. 2.1). In figure 2.10a and 0.8b we present the maps corresponding to the n-HUC and RF methodologies, respectively. Spatial differences arise from the nature of both methods, in the n-HUC interpolation (fig. 2.10a), the spatial distribution holds the shape of the HUCS depending on the density of previously analyzed watersheds. On the other hand, the RF method shows patterns that involve stream magnitude, localization, and watershed characteristics (fig. 2.10b).

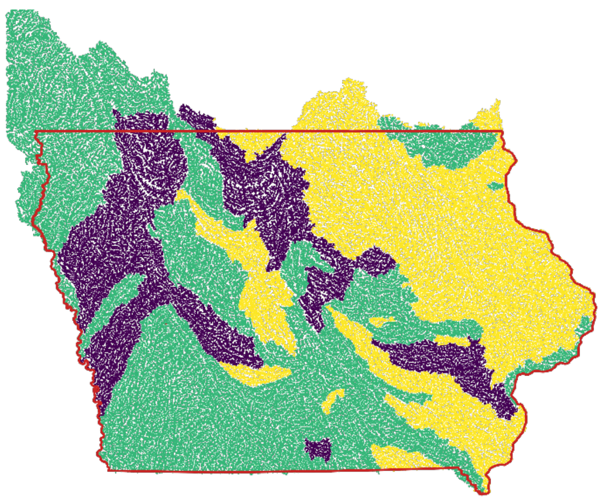

a) n-HUC interpolation.

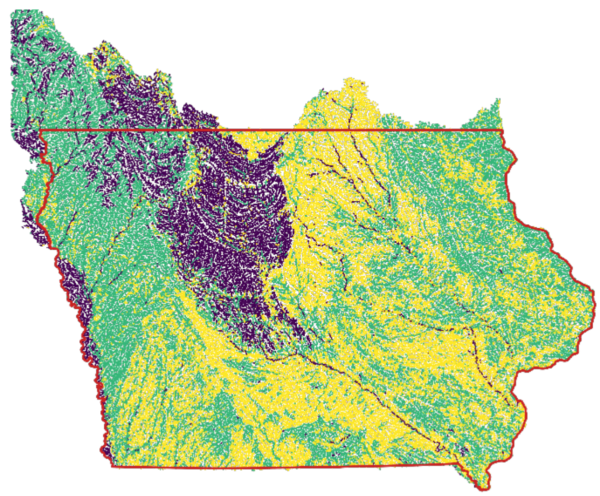

b) Random forest interpolation result.

Figure 2.10 Map result of the λ_1 and v_0 interpolation obtained by the a) n-HUC method and b) by the random forest. Yellow values correspond to $\lambda_1 = 0.2$ and $v_o = 0.3$, green to $\lambda_1 = 0.25$ and $v_o = 0.4$, and purple to $\lambda_1 = 0.15$ and $v_o = 0.2$.

As mentioned in the methodology, for the RF interpolation, we use the best 74 different realizations, and for each link, we select the λ_1-v_0 combination with more occurrences. This method involves a discrepancy and confidence among the multiple RFs. The confidence is high when a high percentage of them select the same λ_1 and v_0, we calculate it as the modal value for the link divided by the total number of RFs (74). In this case, we obtain a relatively good agreement with confidence values oscillating between 0.5 and 0.83 in a vast region of Iowa. Also, the obtained results have a regionalization pattern probably explained by the patterns of some of the input data. The uncertainty of the high-order streams is possibly associated with differences in the information that the RF method has during training and testing (51 small watersheds) contrasted with the information that it uses to predict (all the links).

After the interpolation, we run the HLM-Toplayer model between the years 2012 and 2018. The run of the HLM model has three variations, which are the open loop, the n-HUC, and the RF. The open-loop variation stands for the model with constant parameters λ_1 and v_0 equal to 0.2 and 0.33, respectively. The n-HUC model has the λ_1 and v_0 distribution corresponding to the one presented in figure 2.10a. The RF model, distributed λ_1 and v_0 with the results shown in figure 2.10b. Results show that the KGE performance index is similar between the open-loop and the RF model, and it tends to be lower for the n-HUC model (fig. 2.11).

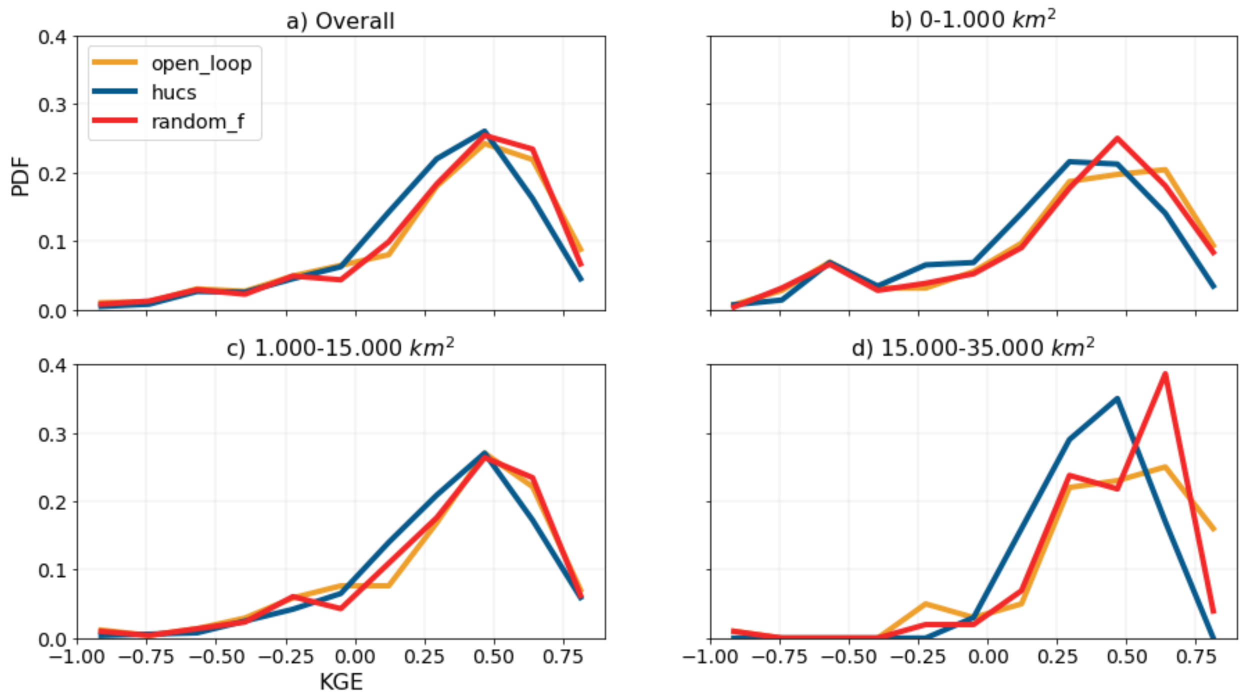

Figure 2.11 KGE index distribution. a) Evaluation for 138 USGS links inside Iowa, b) evaluation for links with areas between 0.1 and 1000 km^2. c) Links with areas between 1000 and 15000 km^2. d) Evaluation for links with areas between 15000 and 35000 km^2.

We also compare the performance of the three models to simulate peak flows. Figure 2.12 presents the comparison between the observed peak-flows (x-axis) and the simulated peak-flows (y-axis). Additionally, in the figure, we present the interquartile band and the median value for different observed intervals. All the models present underestimation for low peak flows. In the cases of the open-loop and RF, this behavior tends to change with the increase of the peak flow value. The open-loop is the model that most tend to overestimate, while the n-HUC tends to underestimate. Moreover, the RF model makes a better approximation of the peak flows. Our results still show a significative dispersion potentially explained by uncertainties at λ_1, v_0, and other parameters of the model not explored in the described experiment.

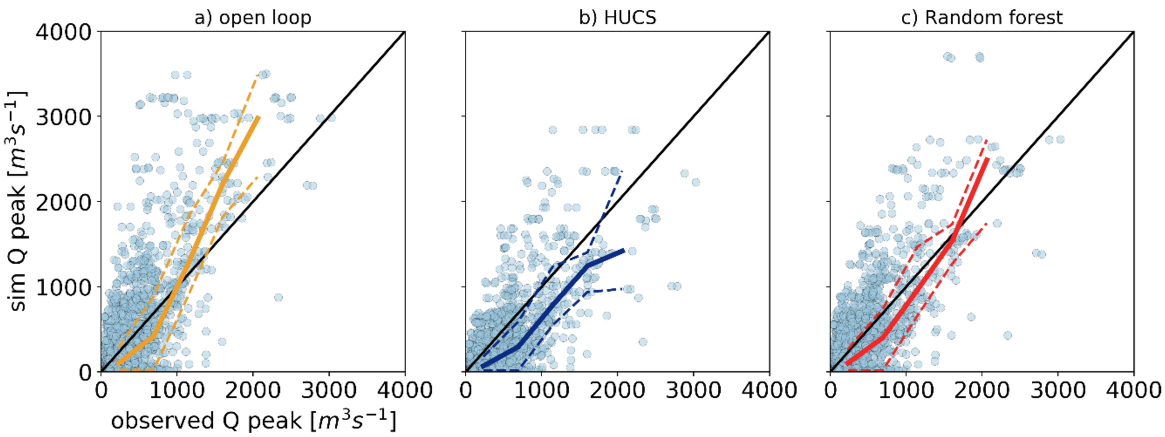

Figure 2.12 Scatter plot of observed peak flows vs simulated peak flows. Red lines correspond to the percentiles of the simulated peak flows for different observed interval.

The simulated peak flows behavior presented in figure 2.12 also applies at multiple scales. According to figure 2.13, the three versions of the model exhibit underestimation for watersheds with areas below 1000 km^2. Besides, there is a relatively good fit for basins with areas between 2000 km^2 and 10,000 km^2. Finally, for large watersheds (above 10,000 km^2), the behavior switches to overestimation. The open-loop model is the model with more overestimations across scales. On the other hand, the RF model seems to present a good peak low performance for scales between 2000 and 10,000 km^2. In contrast, the n-HUC has a slight underestimation for almost all scales except for watersheds with large areas (above 10,000 km^2).

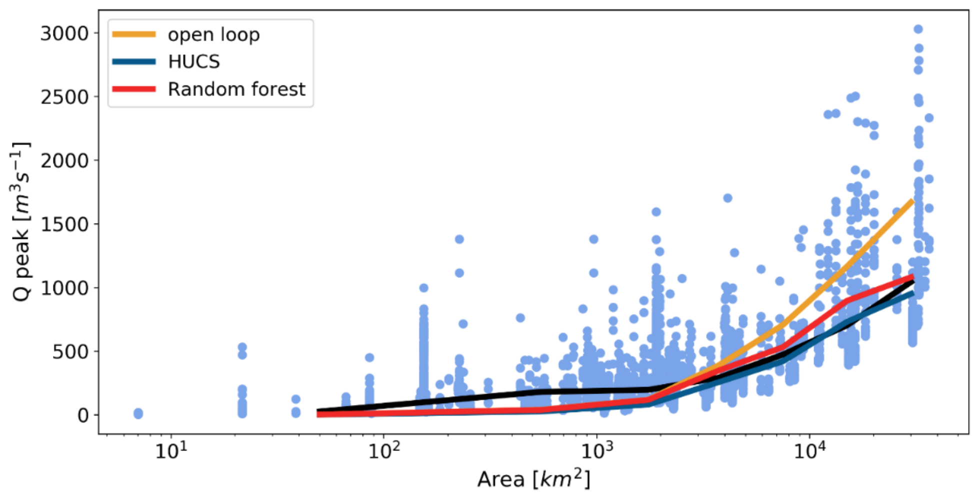

Figure 2.13 50th percentile evolution across scales, the black line corresponds to the observations, and the blue dots to the observed peak flows.

Finally, we analyze the performance of the model setups in terms of the peak flow difference and the time to peak difference (fig. 2.14). The results of the first row, show that the time differences tend to decrease for the RF case for the cases with a peak flow magnitude lower than 50 $m^3 \cdot s^{-1}$. For the remaining magnitudes there is no evident differences. Besides, the peak flow difference shows a lower difference for magnitudes above 300 $m^3 \cdot s^{-1}$ in the case of the RF. The second row also presents a similar result, the RF case has lower peak flow difference for the watersheds with areas above 2600 km2.

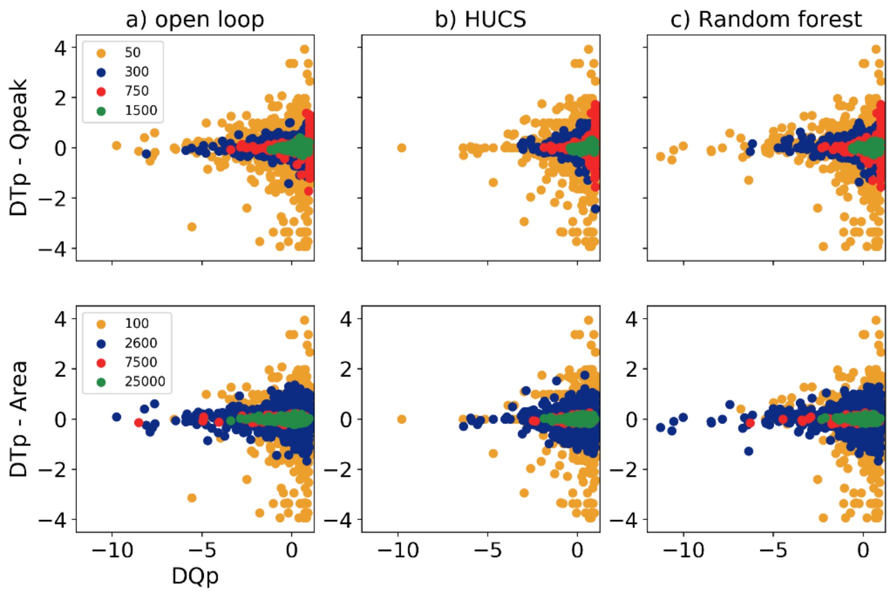

Figure 2.14 Peak flow difference(x-axis) and time peak difference (y-axis) for the different model realizations. The first row, colors the dots in function of the peak flow magnitude. The second row, colors the dots in function of the watershed area.

In this chapter we have presented a novel approach to obtain the parameters for a hydrological model. The approach starts from data of the region corresponding to small watersheds and ends interpolating the results for the model domain. In contrast with a typical calibration procedure, our results represent an advance in the case of ungauged basins in a gauged region. Moreover, we show that it is possible to increase the performance of some objective functions without affecting the overall performance. However, the method seems to be sensitive to the density of the data and the interpolation method. In this case, the random forest methodology has proven to be effective for classification and eventually interpolation. In a future work we expect to expand this methodology to other regions and include more parameters of the model.

Chapter 3 Subsurface flow improvement and tile drainage incorporation

As a part of the effort to improve the model performance, we also work on the model representation of the subsurface and tiles processes. According to several authors (Andrews et al., 2011; Klaus & Zehe, 2010; Loritz et al., 2016; Tallaksen, 1995), a significant portion of the hydrograph came from subsurface flow. In the USA Mid-West, the subsurface flow has been changed by the presence of tile drainage systems (Schilling & Helmers, 2008). Among all the implications of the tile drainage (Dinnes et al., 2002; Holden et al., 2019; Li et al., 2010), this practice also affects the transport times of water at the subsurface, and eventually the shape of the hydrographs (fig. 3.1). However, for us it is important to have a good representation of them on the HLM model. Their inclusion will help to improve the model understanding of the process, and eventually, its performance.

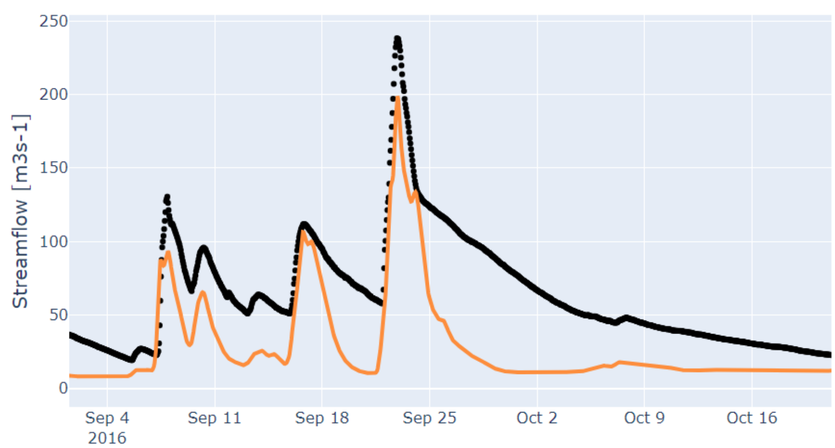

Figure 3.1 Example of a hydrograph (black dots) at West Fork at Cedar River (05458900). To contrast this effect, in orange we present the HLM model results.

3.1 Methodology

We have developed a multi-model methodology to include the subsurface and tiles dynamics into HLM. Our methodology includes first the usage of the physical model Hydrus

CITAS, and then, the implementation of its results into HLM. In the Hydrus model we simulate several setups of virtual hillslopes with tiles and without tiles. Then, we evaluate the results from the different hillslopes and obtain a general equation to describe the hillslope output in function of its storage. Finally, we include in the HLM model one version of the obtained equation and validate the new model for 18 USGS stations at the Cedar River at Bluff (05464780).

The model Hydrus uses the Van Genuchten equations with hysteresis upon refill. Simulations in Hydrus are computed by solving Richard's equations, a PDE model to describe flow through porous media using the finite element method on user-specified elements. Such a method can precisely capture the depth and shape of a water table that is variable in space while also representing the depth-distribution of water in the unsaturated zone of the subsurface. Finally, the outputs of Hydrus include fluxes through different hillslope faces at user-specified precision and total subsurface storage with rougher precision. As we develop a corresponding ODE model, we consider only the total volume of water, ignoring spatial and depth distribution of water concentration.

The hillslope for our simulations is a 40 × 40-meter square prism with a depth of 4 meters (fig. 3.2). The soil type is silty loam with the Hydrus default soil parameters. The top surface of our hillslope experiences atmospheric boundary conditions (including potential evapotranspiration and infiltration), the bottom of the hillslope allows no water transfer, nor do three of the four vertical faces. The final vertical face of the hillslope (the downhill face) undergoes the seepage boundary condition, which means the flow through of this face only occurs in regions of saturation. The flow out of this face is called subsurface flow.

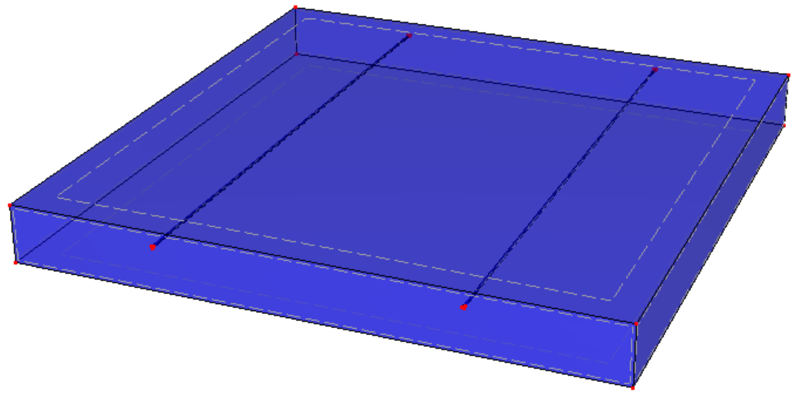

Figure 3.2 Hillslope for Hydrus simulations. For 'drainage simulations' (simulations that include tiles), two tiles are represented, and they run along the gradient of the hillslope. The leftmost face is called the 'seepage face,' while all other vertical faces allow no water transfer. The top face undergoes atmospheric conditions.

Tiles (when present) are 2.5 cm in diameter, which are centered 1 meter below the top surface. In simulations, the tiles also undergo seepage conditions, which is to say that the soil surrounding the tiles must be saturated if they are to be actively draining. Because the tiles are only a meter below the surface, the soil must be near saturation to 'activate' tiles. Although, subsurface drainage tiles are typically only included for poorly drained soils, which usually implies flat terrain. We have run simulations for hillslopes with gradients between 0% and 10%. For higher slopes, the tiles have poor effect over the hillslope outflow, since most of the flow is parallel to them and out of the downhill seepage face.

Each of our simulations represents 1600 days with 400 time-steps reporting seepage and storage. Throughout the simulation, the potential evapotranspiration is set to 1.5 $mm \cdot day^{-1}$ (constant). Since the porosity is 0.45, the soil is initially nearly saturated (uniformly distributed soil water content of 0.43) and allowed to drain as subsurface flow. When soil is not saturated, this is not a realistic representation of a soil moisture profile, so we require that these drainage simulations be over a long enough time period that the soil can achieve a reasonable soil moisture profile as it drains. The hillslope begins nearly saturated, but drains without rainfall for 100 days, priming the hillslope for the first precipitation event by distributing subsurface water into a more realistic profile. During days 100-131, an infiltration pattern based on rainfall from July 1993 is applied. The soil drains, and the same infiltration pattern is applied again beginning on days 300 and 500.

From the results of the Hydrus model we obtain a generic formulation for the outflow subsurface flow in function of the stored water. For this, we first record the results of Hydrus after the 500th time-step. At this point, we record the mean value of the stored water in the hillslope, and the total outflow. Then, we compare the outflow in function of the storage, and graphically compare the results for the multiple setups of the hillslope. Since the curves belong to setups with different slopes, soil depth, and tiles no tiles, they represent curves that oscillate in different ranges, but that show similar behavior. Knowing this, we collapse the curves of each case by standardizing the x and y-axis.

This collapsed curve is mainly defined by three parameters, the no outflow storage S_0, the activation storage S_n, and its exponential parameter b. Before S_n, the relationship between the outflow and the storage is linear, after it, it behaves like an exponential equation. The last step of the methodology consists in obtaining an approximation to those three parameters. The difference between S_n and S_0 (ΔS) is the total active water in the hillslopes of the watershed. We obtain this value from measurements of GRACE (Landerer & Swenson, 2012). For this, we took the GRACE records over the last 12 years (fig. 3.3) and estimate the total active water as the difference between the minimum and maximum record. As a result, we estimate ΔS to be equal to 0.248m, we use this value for the HLM model setup, and to find the observed slope for the linear portion of the outflow.

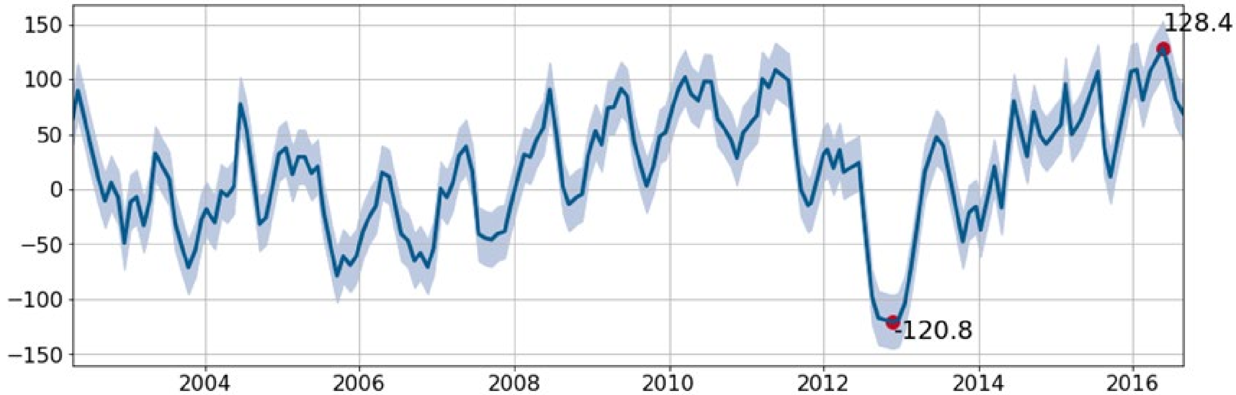

Figure 3.3 GRACE mean anomalies of water stored in the region of Iowa.

To find the linear outflow range, we use the obtained ΔS, and the streamflow records of the USGS stations of the region. Here, we assumed that after a hydrograph event, all the streamflow water is near the activation point S_n, and that the minimum observed record is near S_0. With these assumptions, we extract a time series of the minimum values observed each 4 to 8 weeks. The delta streamflow Δq will be the difference between the maximum value from the series of minimum ($\max_t q_{min}$), and the minimum from the minimum ($\min_t q_{min}$), as presented at equation (3.1). Then, we estimate the outflow rate K_3 by using equation (3.2). Finally, the value implemented in the model is n exponential equation that follows the mean value of the obtained slope for the low flows.

$$\Delta q = \max_t q_{min} - \min_t q_{min} \tag{3.1}$$

$$K_3 = \frac{\Delta q}{\Delta S \cdot A} \tag{3.2}$$

The original setup of the HLM model follows a linear formulation for the subsurface outflow. In the new version, we change this for an exponential formulation (eqn. (3.3). This formulation follows the adjustment for the tiled cases obtained by Hydrus, and for its implementation we seek a curve that follows the parameters obtained at equations (3.1 and (3.2.

$$q_{sL} = aS_s e^{bS_s} \tag{3.3}$$

3.2 Results

We have different setups for the Hydrus model, each setup includes differences in the hillslope depth, slope, and presence of tiles. In figure 3.4 we present a graphical example of the states at two hillslopes, with tiles and without tiles. From each setup, we obtain the relation between the storage and the outflow (fig. 3.5a). Moreover, considering all the cases we obtain a collection of collapsed curves (fig. 3.5b) that show a similar behavior for conditions under the activation point.

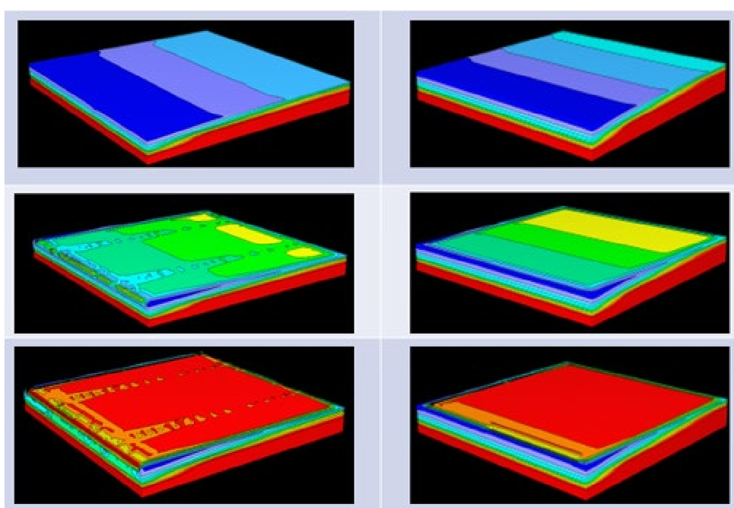

Figure 3.4 Graphical example of the results obtained by Hydrus at a tiled hillslope (left column) and a no tiled hillslope (right column). From top to bottom each row represent a snapshot of the water stored in the model at increasing time intervals.

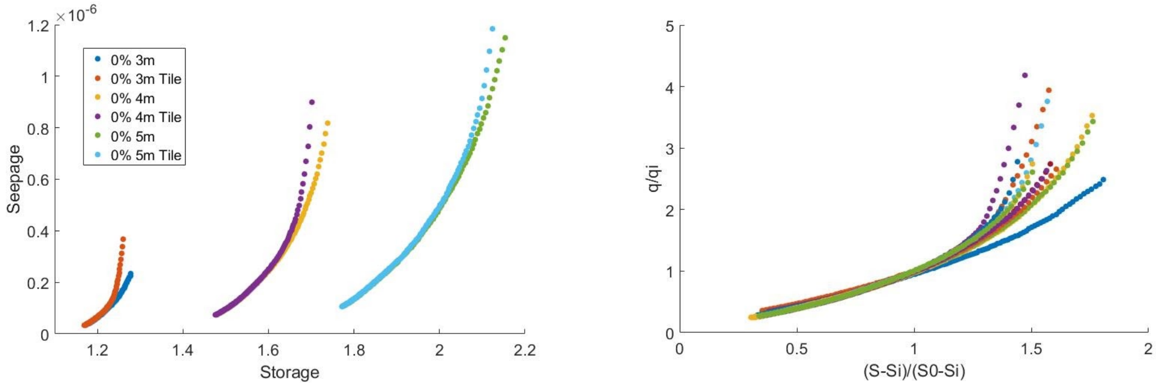

a) Outflow for hillslopes with different depths.

b) Collapsed case of the results obtained at different hillslopes setups.

Figure 3.5 Outflow in function of the storage obtained by Hydrus. (a) Results of three hillslopes with different depths and tiles/no tile case. (b) Collapsed cases standardizing by the activation point and the activation streamflow.

From the collapsed curve we obtain a general shape of the curve and implemented it into the HLM model. For this case, we run the modified HLM model at the Cedar River watershed at Bluff (fig. 3.6a). Cedar River is a watershed that has streamflow records affected by tiles, and also has regions with no tiles (fig. 3.6b). Besides, the watershed has multiple observation sites with good quality records.

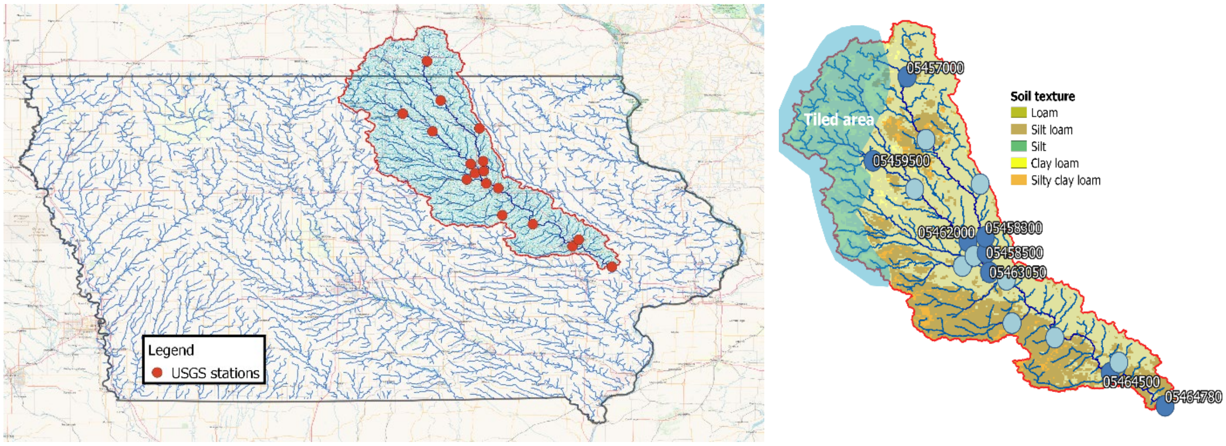

a) Localization of the Cedar River watershed at Bluff.

b) Soils description of the watershed, and tiled region.

Figure 3.6 Localization of the Cedar River watershed at Bluff (a). And soils and tiles description of the watershed (b).

To test the HLM-Tiles model we run it with Stage 4 rainfall from 2012 to 2018. To setup the model we use the river network that IFC uses for the operational model, and for the parameters of the model we use the results obtained by Hydrus. In figure 3.7b we present the mean KGE performance of the model compared with the Toplayer model (fig. 3.7a). According to the figure, with this new setup we achieve to increase the overall performance of the model for the watershed of Cedar River at Bluff. However, there are still streamflow stations at which the model fails to obtain a good representation.

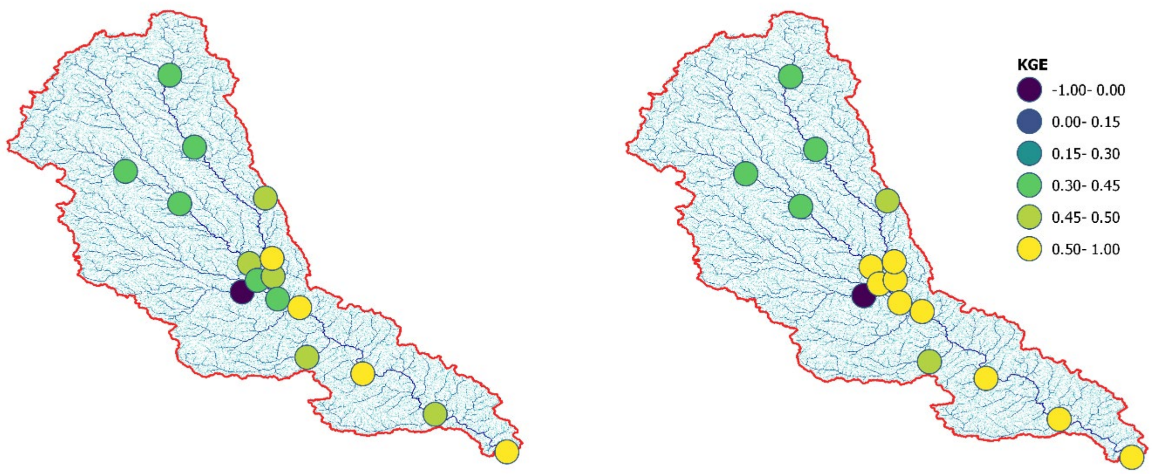

a) HLM-Toplayer model performance
b) HLM-Tiles model performance

Figure 3.7 HLM model KGE performance considering the original setup (a) and the tiles modification (b).

In addition to the performance, we present the simulated streamflow of both models for several stations in figure 3.8. According to the results, the HLM-Tile model achieves to obtain a better representation of the baseflow and the recession curve for almost all cases. The improvement is more evident in the case of the Winnebago River (05459500), which is a highly tailed watershed. In this case, the model achieves an overall good representation. Besides, the improvement improves not only the recession, but also the ascending limb of the hydrograph. However, there are regions in which the tiles assumption tends to make the model overestimate the recession curve (054620000).

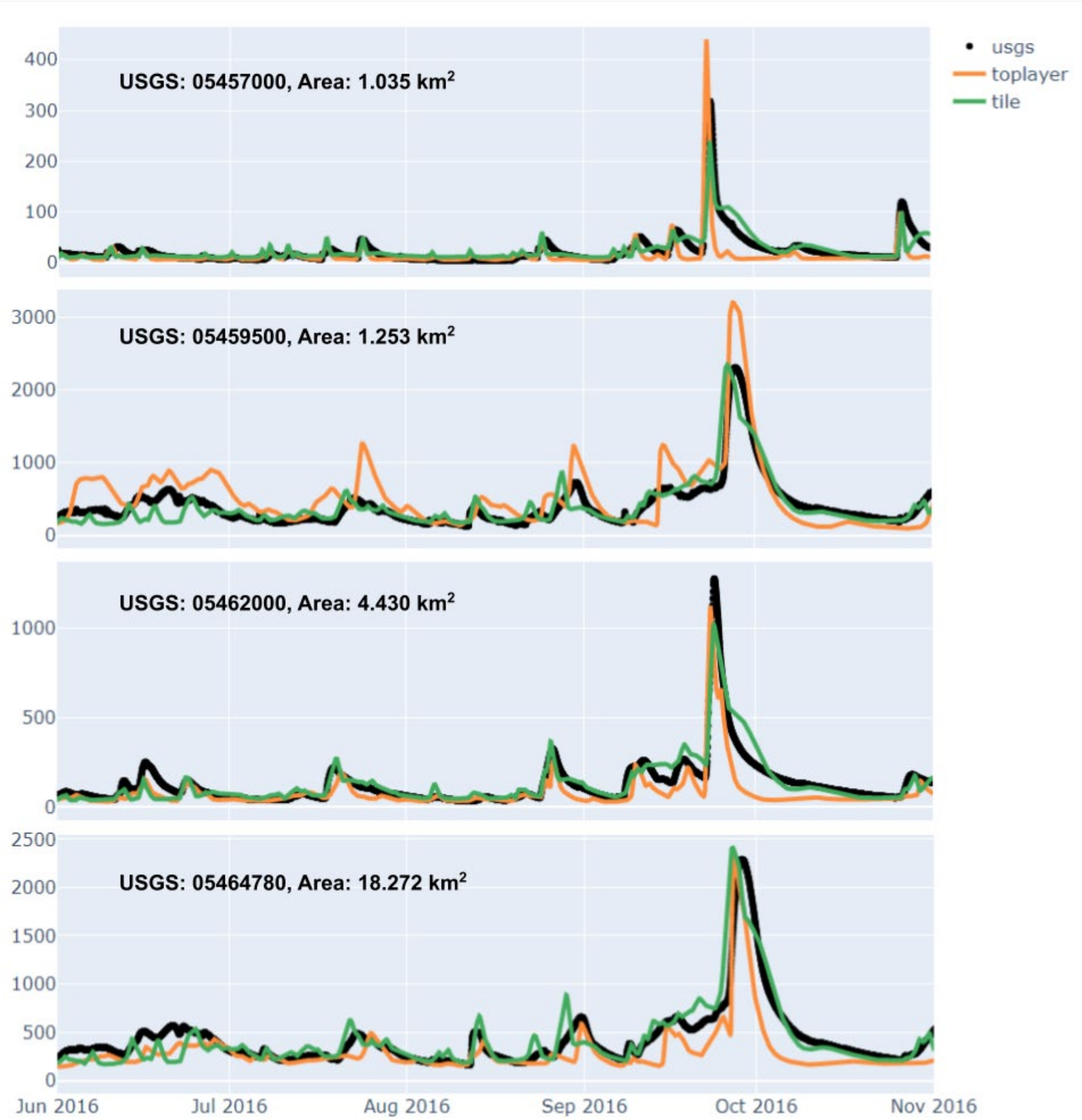

Figure 3.8 Model results at different USGS stations inside the Cedar River watershed at Bluff.

Our results show that the HLM model could be effectively improved by a non-linear representation of the subsurface flow at the hillslopes. Considering the differences between land uses, soil types, and the presence of tiles, this new approach potentially could be extended to large regions. In this case, we assume a tiled representation for all the domain for the case of the

Cedar River at Bluff. With this assumption we achieve to obtain a good representation of the events at some stations, however, there are places with overestimation of the recession.

Chapter 4 Downstream data assimilation.

Streamflow data was forced into HLM by altering the initial conditions of the ordinary differential equation representing the flux in the channel. The state that represents the flux in the channel is initialized with observed values. The change in the initial conditions only takes place on those links where a streamflow gage is located every time new observations are available. The channels upstream of the assimilation point do not get affected. The channels downstream of the gages with observed data get affected because assimilated data is routed downstream with HLM.

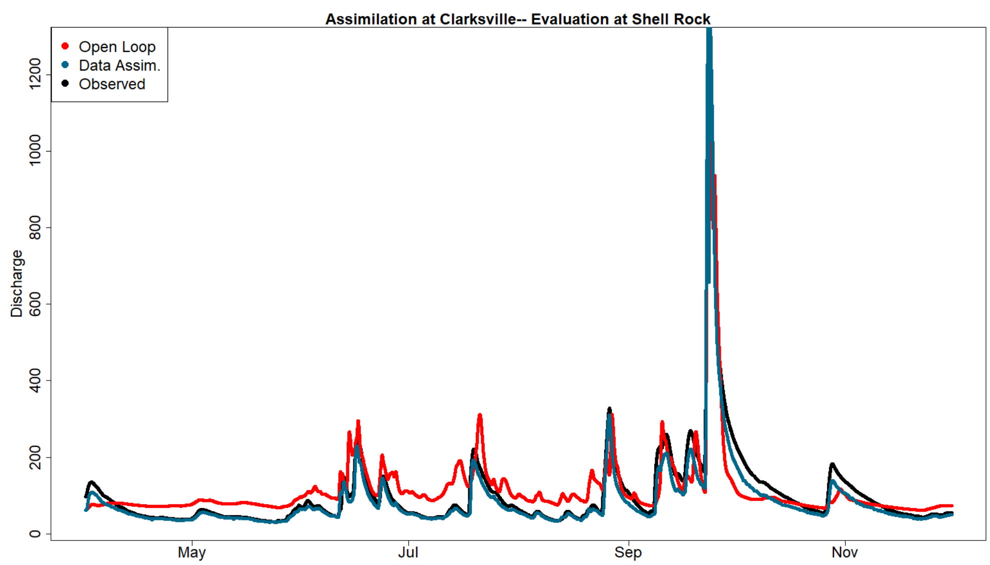

Figure 4.1 Results of the data assimilation at Clarksville. Open loop results (red), data assimilation (blue), observations (black).

In figure 4.1 we present the result for this strategy at the Clarksville station (fig. 4.2). According to the results the strategy improves the model performance, since it transits downstream the amount of water observed upstream. However, the strategy still has some limitations. Its performance depends on the distance of the upstream record. Besides, the methodology could only be applied to regions with records upstream, and the improvement window is limited to the transit time of each watershed. On the other hand, this strategy has proven to be useful improving the performance of the model at regions with a good density of stations.

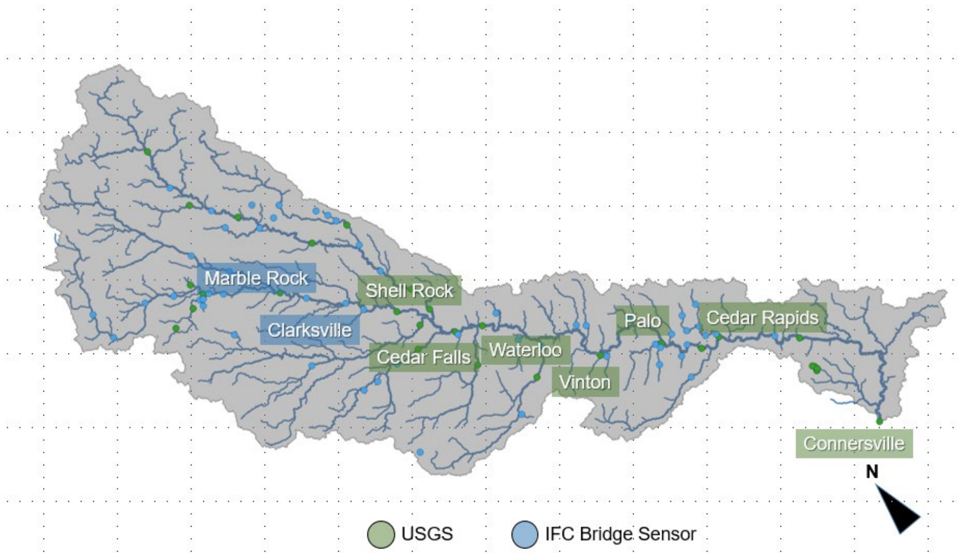

Figure 4.2 Map showing the stations of the assimilation experiment.

Chapter 5 Implementation of a comprehensive evaluation system

We developed a non-proprietary open-source software (NPOSS) that allows users to visualize and analyze multivariate space-time hydrologic data. Hydro-NPOSS leverages the concept of three-dimensional data cubes which allows users to query data in space, time, and variable dimension(s). We implement this concept without requirement of a database system. Thereby, users can define data sources from local file systems and or external data sources (e.g. online data services). This capability makes NPOSS a flexible and portable solution where users can publish their hydrologic datasets in Open Data journals or as companions to their publications. We present example use cases including hydrologic model visualization and evaluation in hindcast and forecast modes for this project.

5.1 Methodology

Hydro-NPOSS consists of three main components: Modules, Configuration, and Graphical User Interface (GUI). Modules are defined as internal libraries and external web tools and technologies. Internal libraries, designed for independent tasks, include functions responsible of extension and orchestration of embedded tools. These tasks are data acquisition, visualization, and user interactions with GUI. External tools/libraries are the open-source web tools that Hydro-NPOSS leverages them. Table 1 summarizes the usage and reference for external libraries used.

Table 5.1 External software used by Hydro-NPOSS

JS LIBRARY	USAGE IN HYDRO-NPOSS	REFERENCE
Leaflet.js	Map and spatial visualizations	https://github.com/Leaflet/Leaflet
Plotly.js	Time-series visualization	https://github.com/plotly/plotly.js
Jquery.js	Creating forms	https://github.com/jquery/jquery
	Data acquisition	
D3.js	Data acquisition	https://github.com/d3/d3
Papaparse.Js	Data acquisition	https://github.com/mholt/PapaParse
Jszip.js	Uzipping data	https://github.com/Stuk/jszip
Moment.Js	Date and Time format	
Math.js	Mathematical operations	https://github.com/josdejong/mathjs
Numeric.js	Numerical analysis	https://github.com/sloisel/numeric
Togeojson.js	Spatial data conversion	https://github.com/tmcw/togeojson

Configuration is a set of information about data sources, metadata, control elements in GUI, and styling of the visualizations. To decrease the effort in deployment, we have created an interactive configuration step in which the user provides the required information using reactive web forms. This information is stored in the configuration file that could be reused by the user without repeating the configuration step. The GUI consists of a map, a visualization canvas for time series, and control elements that are responsible for navigating data. The workflow of

Hydro-NPOSS is shown in figure 5.1. The elements with white and gray background correspond to pre-deployment and post-deployment stages, respectively.

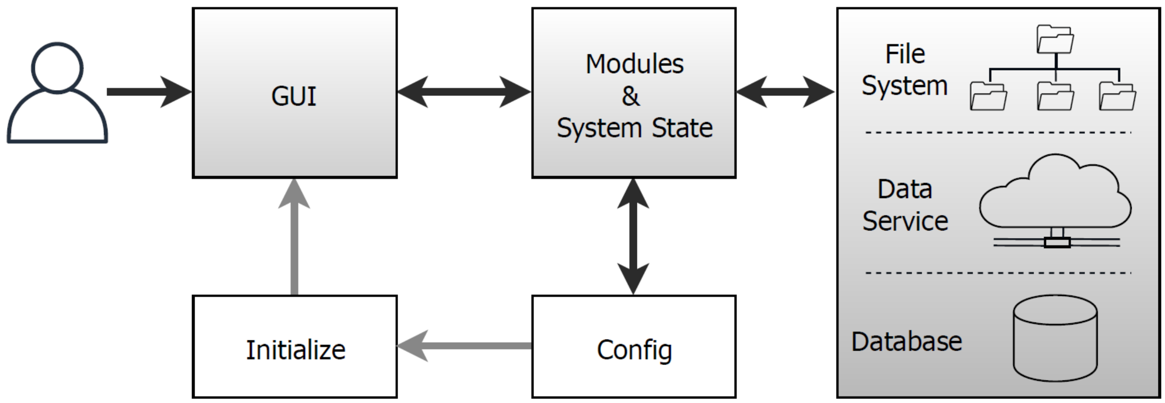

Figure 5.1 Schematic of Hydro-NPOSS workflow.

In the post-deployment step, user interactions are passed to modules by control elements in GUI. Thereafter, modules use configuration information to access data. This step is handled by a Dynamic Path Creator (DPC) as a module that dynamically creates the path to requested data source using the event that corresponds to specific location in the data or element of the data cube. Hydro-NPOSS adopts the concept of data cubes as its data model. Initially, data cubes are introduced by Gray et al. (1997) for reducing the dimensions of the data based on the query that the user requests. Maidment (2002) introduced space-time-variable cube for referencing the individual data to corresponding attributes. Further, Goodall et al. (2008) implemented this concept in integrating time series from different sources for National Water Information System (NWIS).

5.2 Results

We have uploaded the results from Chapter 2 into an implementation of the Hydro-NPOSS software. Figure 5.2 presents a graphical deploy of Hydro-NPOSS showing the KGE.

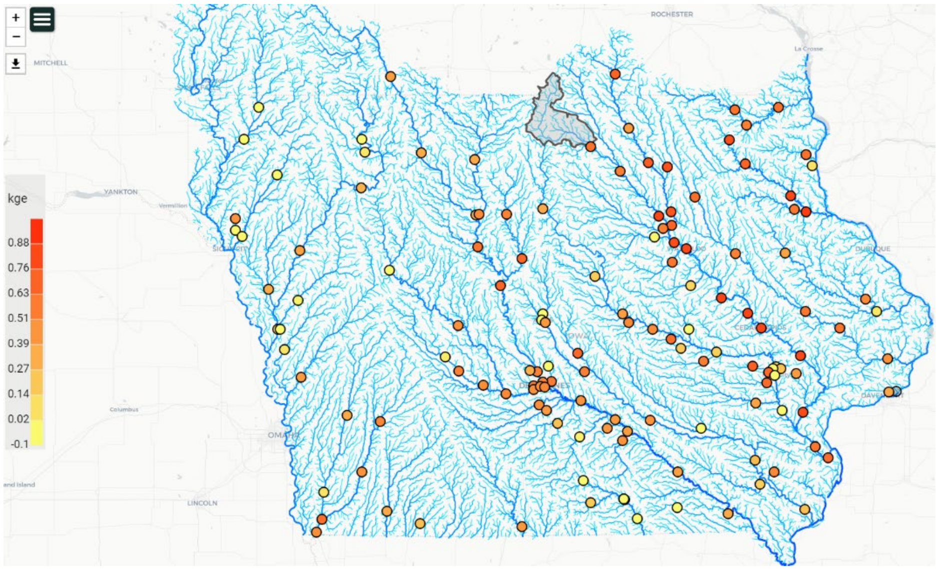

Figure 5.2 Hydro-NPOSS deploying the results obtained with the HLM-Random forest implementation presented at Chapter 2.

The platform also lets the user include different performance indexes and properties of the stations. In this sense, it allows a fast comparison between models and observed data. Figure 5.3 presents the results obtained with the HLM model in Chapter 2 for a watershed inside the area of analysis.

Here is a link to the described web platform; in it we have uploaded the simulation results described in Chapter 2.

http://s-iihr55.iihr.uiowa.edu/hygis.html?config=http://s-iihr51.iihr.uiowa.edu/hydro-analytics.net/evp_experiment/evp.config

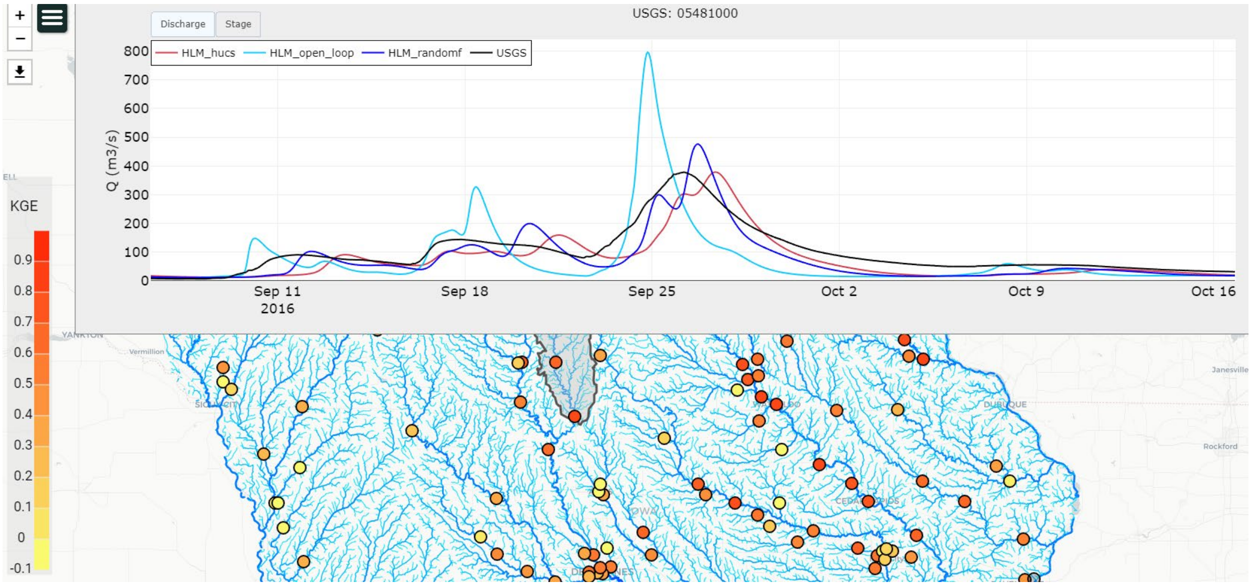

Figure 5.3 Results of the HLM model for the USGS station 05481000. The results belong to the HLM setups described as the open-loop, random forest and n-HUCS at Chapter 2.

Chapter 6 Conclusions

An important aspect in providing a safe, efficient, and effective transportation system is anticipating natural hazards that can lead to road closures. Extreme floods can lead to bridge overtopping and/or compromising the structural integrity of river overpasses, including box culverts. The flood forecasting model and information system proposed here provides a tool to anticipate potential hazardous situations related to floods. It would allow time for the activation of action plans to minimize the impact on the overall transportation system. The forecasting model can be used in real time to anticipate floods and to look at past flooding scenarios to determine if all the actions taken were appropriate or can be improved. Our forecasting system will contribute to improving safety and minimizing risk associated with increasing multi-modal freight movements on the U.S. surface transportation system by *enhancing safety* and providing warning of potential road closures.

As part of this project, we have provided a prototype forecasting web platform with four specific innovations. 1) Forecasts at critical river/road intersections, 2) Spatial animated maps of flood evolution into the future, and 3) a measure of forecast accuracy at the newly incorporated forecast bridges. Our developments give us confidence that we can continue moving forward in developing a forecasting system that is transferable to other locations in the Midwest. As floods continue to be the most costly disaster in the nation, it becomes critical that tools are develop to better predict them.

References

Ali, J., Khan, R., Ahmad, N., & Maqsood, I. (2012). Random Forests and Decision Trees. *International Journal of Computer Science Issues*, *9*(5), 272–278.

Andrews, F. T., Croke, B. F. W., & Jakeman, A. J. (2011). An open software environment for hydrological model assessment and development. *Environmental Modelling and Software*, *26*(10), 1171–1185. https://doi.org/10.1016/j.envsoft.2011.04.006

Ayalew, T., Krajewski, W., Mantilla, R. (2013). Exploring the Effect of Reservoir Storage on Peak Discharge Frequency. J. Hydrol. Eng. 18, 1697–1708. https://doi.org/10.1061/(ASCE)HE.1943-5584.0000721

Ayalew, T. B., Krajewski, W. F. & Mantilla, R. (2014), “Connecting the power-law scaling structure of peak-discharges to spatially variable rainfall and catchment physical properties,” *Advances in Water Resources*, vol. 71, pp. 32–43.

Ayalew, T., Krajewski, W., Mantilla, R. (2015). Insights into Expected Changes in Regulated Flood Frequencies due to the Spatial Configuration of Flood Retention Ponds. J. Hydrol. Eng. 20, 4015010–4015010. https://doi.org/10.1061/(ASCE)HE.1943-5584.0001173

Ayalew, T.B., Krajewski, W.F., Mantilla, R., Wright, D.B., Small, S.J. (2017). Effect of Spatially Distributed Small Dams on Flood Frequency: Insights from the Soap Creek Watershed. J. Hydrol. Eng. 22. https://doi.org/10.1061/(ASCE)HE.1943-5584.0001513

Bhatt, Gopal et al. (2014) (https://pdfs.semanticscholar.org/715d/d10d9c3a356ef61c576bf1afb8f704bfd0ca.pdf)

Breiman, L. (1994). Bagging predictors: Technical Report No. 421. *Department of Statistics University of California*, *2*, 19. https://www.stat.berkeley.edu/~breiman/bagging.pdf

Choi, C. C., Constantinescu, G., & Mantilla, R. (2015). Implementation of a Hydraulic Routing Model for Dendritic Networks with Offline Coupling to a Distributed Hydrological Model. Journal of Hydrologic Engineering.

Cunha, L.K., P.V. Mandapaka, W.F. Krajewski, R. Mantilla, and A.A. Bradley. (2012). Impact of radar rainfall error structure on estimated flood magnitude across scales: An investigation based on a parsimonious distributed hydrological model, Water Resources Research, 48(10), W10515.

Devia, G. K., Ganasri, B. P., & Dwarakish, G. S. (2015). A Review on Hydrological Models. *Aquatic Procedia*, *4*(Icwrcoe), 1001–1007. https://doi.org/10.1016/j.aqpro.2015.02.126

Dinnes, D., Jaynes, D. B., Kaspar, T., & Hatfield, J. (2002). Nitrogen Management Strategies to Reduce Nitrate Leaching in Tile-Drained Midwestern Soils PhD research project on soil desinfection with ozone in substitution to synthetic pesticides View project Enhancing Soil Begins with Soil Biology and a Stable Soil Microclimate View project. *Article in Agronomy Journal*, *December 2014*. https://doi.org/10.2134/agronj2002.0153

Goodall, J. L., Horsburgh, J. S., Whiteaker, T. L., Maidment, D. R., & Zaslavsky, I. (2008). A first approach to web services for the National Water Information System. *Environmental Modelling and Software*, *23*(4), 404–411. https://doi.org/10.1016/j.envsoft.2007.01.005

Gray, J., Chaudhuri, S., Bosworth, A., Layman, A., Reichart, D., Venkatrao, M., Pellow, F., & Pirahesh, H. (1997). Data cube: A relational aggregation operator generalizing group-by, cross-tab, and sub-totals. *Data Mining and Knowledge Discovery*, *1*(1), 29–53. https://doi.org/10.1023/A:1009726021843

Gupta, H. V., Kling, H., Yilmaz, K. K., & Martinez, G. F. (2009). Decomposition of the mean squared error and NSE performance criteria: Implications for improving hydrological modelling. *Journal of Hydrology*, *377*(1–2), 80–91. https://doi.org/10.1016/j.jhydrol.2009.08.003

Gupta VK, Waymire EC. (1998). Spatial Variability and Scale Invariance in Hydrologic Regionalization. In Scale Dependence and Scale Invariance in Hydrology, Sposito G (ed.).Cambridge University Press: Cambridge; 88–135. DOI: 10.1017/CBO9780511551864.005

Holden, J., Chapman, P. J., Kay, P., Mitchell, G., & Pitts, C. S. (2019). Surface water quality. *Water Resources*, 99–150. https://doi.org/10.4324/9780429448270-4

Kam Ho, T. (1995). Random Decision Forests Perceptron training. *AT&T Bell Laboratories*.

Klaus, J., & Zehe, E. (2010). Modelling rapid flow response of a tile-drained field site using a 2D physically based model: Assessment of “equifinal” model setups. *Hydrological Processes*, *24*(12), 1595–1609. https://doi.org/10.1002/hyp.7687

Krajewski, W.F., A. Kruger, S. Singh, B.-C. Seo and J.A. Smith, Hydro-NEXRAD-2: Real-time access to customized radar-rainfall for hydrologic applications, Journal of Hydroinformatics, 15(2), 580-590, 2013.

Krajewski, W. F., Ceynar, D., Demir, I., Goska, R., Kruger, A., Langel, C., Young, N. C. (2017). Real-time flood forecasting and information system for the state of Iowa. Bulletin of the American Meteorological Society, 98(3), 539–554. https://doi.org/10.1175/BAMS-D-15-00243.1

Landerer, F. W., & Swenson, S. C. (2012). Accuracy of scaled GRACE terrestrial water storage estimates. *Water Resources Research*, *48*(4), 1–11. https://doi.org/10.1029/2011WR011453

Laplante and Phillip. (2007). What Every Engineer Should Know About Software Engineering.

Li, H., Sivapalan, M., Tian, F., & Liu, D. (2010). Water and nutrient balances in a large tile-drained agricultural catchment: A distributed modeling study. *Hydrology and Earth System Sciences*, *14*(11), 2259–2275. https://doi.org/10.5194/hess-14-2259-2010

Loritz, R., Hassler, S. K., Jackisch, C., Allroggen, N., van Schaik, L., Wienhöfer, J., & Zehe, E. (2016). Picturing and modelling catchments by representative hillslopes. *Hydrology and Earth System Sciences Discussions*, 1–56. https://doi.org/10.5194/hess-2016-307

Maidment, D. R. (2002). Arc Hydro: GIS for water resources. In *Agriculture*.

Mantilla, R. and V.K. Gupta, (2005). A GIS numerical framework to study the process basis of scaling statistics in river networks, IEEE Geoscience and Remote Sensing Letters, 2(4), 404-408.

Mantilla, R., Gupta, V. K. & Mesa, O. J. (2006).Role of coupled flow dynamics and real network Mantilla, R. (2007). Physical basis of statistical self-similarity in peak flows on random self-similar networks, PhD dissertation, University of Colorado, Boulder.

Mantilla, R. (2007). Physical basis of statistical self-similarity in peak flows on random self-similar networks, PhD dissertation, University of Colorado, Boulder.

Mantilla, R., Cunha, L. K., Krajewski, W. F., Small, S. J., Jay, L. O., Fonley, M. & Curtu, R. (2012), "Simulation of a Distributed Flood Control System using a Parallel Asynchronous Solver for Systems of ODEs," Applied Simulation and Modeling, June, Napoli, Italy, http://dx.doi.org/10.2316/P.2012.776-042.

Moser, B. A., Gallus, Jr., W. A., & Mantilla, R. (2015). An Initial Assessment of Radar Data Assimilation on Warm Season Rainfall Forecasts for Use in Hydrologic Models. Weather and Forecasting, vol. 30, no. 6, pp. 1491-1520.

Moussa, R., Chahinian, N., & Montpellier, H. (2009). Comparison of different multi-objective calibration criteria using a conceptual rainfall-runoff model of flood events. *Earth*, 519–

535.

Newton, D.W., and Herrin, J.C. (1982). Assessment of commonly used methods of estimating flood frequency, Transportation Research Record, 896, 10-30.

NWS – National Weather Service. Climate Reports: August 2016 & summer 2016. [Online] 2016. http://www.weather.gov/dvn/Climate_Monthly_08_2016 (accessed Mar 21, 2017).

Pedregosa, F., Varoquaux, G., Gramfort, A., Michel, V., Thirion, B., Grisel, O., Blondel, M., Prettenhofer, P., Weiss, R., Dubourg, V., Vanderplas, J., Passos, A., Cournapeau, D., Brucher, M., Perrot, M., & Duchesnay, E. (2012). Scikit-learn: Machine Learning in Python. *Journal of Machine Learning*, *12*, 2825--2830.

Quinlan, J. R. (1986). Induction Fo Decion Trees. *Machine Learning*, *1*, 81–106.

Sasaki, Y. (2007). The truth of the F-measure. *Teach Tutor Mater*, 1–5. http://www.cs.odu.edu/~mukka/cs795sum09dm/Lecturenotes/Day3/F-measure-YS-26Oct07.pdf

Schilling, K. E., & Helmers, M. (2008). *Effects of subsurface drainage tiles on streamflow in Iowa agricultural watersheds : Exploratory hydrograph analysis*. *4506*(May), 4497–4506. https://doi.org/10.1002/hyp

Seo, B.-C., W.F. Krajewski and L.K. Cunha, Impact of radar-rainfall uncertainty on hydrologic response for the eastern Iowa flood of 2008, Water Resources Research, 49, 2747–2764, 2013.

Small, S. J., Jay, L. O., Mantilla, R., Curtu, R., Cunha, L. K., Fonley, M., & Krajewski, W. F. (2013). An asynchronous solver for systems of ODEs linked by a directed tree structure. Advances in Water Resources, 53, 23–32. https://doi.org/10.1016/j.advwatres.2012.10.011

Sivapalan, M. (2018). From engineering hydrology to Earth system science: Milestones in the transformation of hydrologic science. *Hydrology and Earth System Sciences*, *22*(3), 1665–1693. https://doi.org/10.5194/hess-22-1665-2018

State of Iowa. (2009). https://www.legis.iowa.gov/docs/ico/section/466C.1.pdf

Tallaksen, L. M. (1995). A review of baseflow recession analysis. *Journal of Hydrology*, *165*(1–4), 349–370. https://doi.org/10.1016/0022-1694(94)02540-R